Experimental determination of the resistance of a single-axis solar tracker to torsional galloping

Eva Martínez García[1a], Eduardo Blanco Marigorta[1b], Jorge Parrondo Gayo[1b] and Antonio Navarro-Manso[*1]

[1]*Department of Energy, University of Oviedo, Engineering Polytechnic School of Gijón, C/ Wifredo Ricart, s/n, Edificio Departamental Este, Campus Universitario de Viesques, 33204 Gijón, Asturias, Spain*

(Received keep as blank , Revised keep as blank , Accepted keep as blank)

Abstract. One of the most efficient designs of solar trackers for photovoltaic panels is the single-axis tracker, which holds the panels along a torque tube that is driven by a motor at the central section. These trackers have evolved to become extremely slender structures due to mechanical optimization against static load and the need of cost reduction in a very competitive market. Owing to the corresponding decrease in mechanical resistance, some of these trackers have suffered aeroelastic instability even at moderate wind speeds, leading to catastrophic failures. In the present work, an analytical and experimental approach has been developed to study that phenomenon. The analytical study has led to identify the dimensionless parameters that govern the motion of the panel-tracker structure. Also, systematic wind tunnel experiments have been carried out on a 3D full aeroelastic scale model. The tests have been successful in reproducing the aeroelastic phenomena arising in real-scale cases and have allowed the identification and a close characterization of the phenomenon. The main results have been the determination of the critical velocity for torsional galloping as a function of tilt angle and a calculation methodology for the optimal sizing of solar tracker shafts.

Keywords: single-axis tracker, wind load, aeroelastic model, torsional galloping, stability diagram, wind tunnel

1. Introduction

Nowadays a wide-spread trend in the sector of solar photovoltaic farms is the use of single-axis solar trackers with one degree of freedom (Lave and Kleissl 2011). According to the common design of these trackers, the solar panels are held along a horizontal torque tube that can rotate up to a finite angle about a vertical axis by means of a motor located at the central section. Hence, this system allows to control the azimuth but not the altitude. Although the energy obtained is lower than with a two-degree-of-freedom solar tracker, it is still 30% higher than the one obtained with fixed solar panels (Talavera *et al.* 2019).

The structural arrangement of these solar trackers consists in several solar panels aligned on a torsional shaft. The shaft is supported by several pillars that allow only for rotational motion. One end of the shaft is free, and the other one is fixed to a gearmotor (driver) that controls the angular position. Usually, these structures are symmetrical about the driver, with a row of panels at each side. Fig. 1 shows an example of structural scheme for this type of solar tracker.

Due to the progressive mechanical optimization against static loads and non-extreme accidental events, plus the continuous search for cost reduction in a very competitive market as the photovoltaic sector, those structures have evolved to become very slender. In the last years, however, that has led to multiple cases of aerolastic instability phenomena under different conditions (Taylor and Browne 2020), which are attributed to torsional galloping, flutter or torsional divergence.

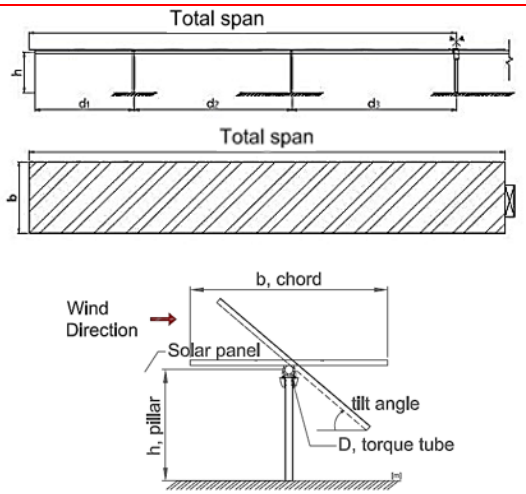

Fig. 1 Scheme of the single-axis solar tracker

Frequently, those aerolastic phenomena provoke the failure of the structure. Components commonly subjected to

[*]Corresponding author, Ph.D. Professor
E-mail: navarroantonio@uniovi.es

[a]Ph.D. Student
[b]Ph.D. Full Professor

fatigue and collapse are the positioning motor, the driver supports and the main shaft, though the solar panels become frequently destroyed as well (Fig. 2).

Fig. 2 Collapse of a single-axis solar tracker facility (rendering)

While current construction standards are intended to account for basic aeroelastic effects (Blevins 1990, Païdoussis et al. 2011) by means of dynamic amplification factors (Dyrbye and Hansen 1997, Taylor and Browne 2020), it is clear that they are not capable to include the specific effects of wind on single-axis trackers with solar panels. Indeed, an appropriate calculation of these structures has to be based on a deeper understanding of the aeroelastic phenomena involved, which usually requires wind tunnel tests (Taylor and Browne 2020).

Many studies have been conducted on the aerodynamics of flat plates, including analytical (Yang 2010), computational (Jubayer and Hangan 2015) and experimental methodologies (Strobel and Banks 2014). The object of study has ranged from the case of panels with single-degree-of-freedom models to complete photovoltaic farms with panels on solar trackers. The latter have usually been designed with static models in order to study the effect of wind directionality and the resulting interferences between different rows of trackers. However, few investigations have been based on full aeroelastic tests (Roedel and Upfill-Brown 2018).

Following that line of work, this paper presents a new study intended to develop a method of analysis and calculation of the mechanical characteristics of solar panel trackers that allows avoiding structure failures due to aeroelastic phenomena. As the state of knowledge for that structure typology is still at an early phase (Rhor *et al*. 2015), this study began with an inspectional analysis of the differential equation for shaft torsional motion, so that appropriate non-dimensional parameters could be established for both aerodynamic and structural phenomena. Similarity conditions were then applied for the design of small scale models of solar panel trackers with full aeroelastic characteristics. Then, wind tunnel tests were extensively conducted under a variety of conditions.

As expected, several aeroelastic phenomena were observed, including vibrations induced by vortex shedding, torsional galloping or flutter. The main results obtained can be summarized as:

- Physical explanation of the aeroelastic phenomena causing instability in the solar tracker structure.
- Determination of the critical velocities for different tilt angles (azimuthal orientation).
- Proposal of a safe design criterion for the analyzed case in terms of project wind velocities and structure rigidity.

2. Methodology

2.1 Non-dimensional analysis

Nine variables were initially considered to configure the flow-structure system that represents solar panel trackers with a given geometrical pattern. Three of them correspond to the flowing fluid: upstream velocity, density and viscosity (U, ρ, μ). Four are related to the structure: characteristic length (L) - typically span or chord -, torsional stiffness (K), moment of inertia with respect to the shaft axis (I), and structural damping (c). The last variables refer to the aerodynamic forces, which in this case can be reduced to a torque magnitude (T) and an excitation frequency (ω).

The variables corresponding to the fluid and the aerodynamic forces lead to the usual dimensionless numbers of torque coefficient (C_T), in this case as the moment coefficient, Strouhal number (St) and Reynolds number (Re), Eqs. (1)-(3)

$$C_T = \frac{T}{\frac{1}{2}\rho U^2 L^3} \tag{1}$$

$$St = \frac{\omega L}{U} \tag{2}$$

$$Re = \frac{\rho U L}{\mu} \tag{3}$$

Non-dimensional numbers that collect the properties of the structure can be derived from the equation of torsional motion as given by Eq. (4), where θ is the angular displacement:

$$I\frac{d^2\theta}{dt^2} + c\frac{d\theta}{dt} + K\theta = T \tag{4}$$

Analysis of Eq. (4) brings about three dimensionless parameters, which can be formulated as a torsional stiffness coefficient (C_K), a reduced natural frequency (ω^*) and the damping ratio (ξ), i.e. the ratio between structural and critical damping (Eqs. (5)-(7)).

$$C_K = \frac{K}{{}^1\!/_2\,\rho U^2 L^3} \tag{5}$$

$$\omega^* = \frac{L}{U}\sqrt{{}^K\!/_I} \tag{6}$$

$$\xi = \frac{c}{2\sqrt{(KI)}} \tag{7}$$

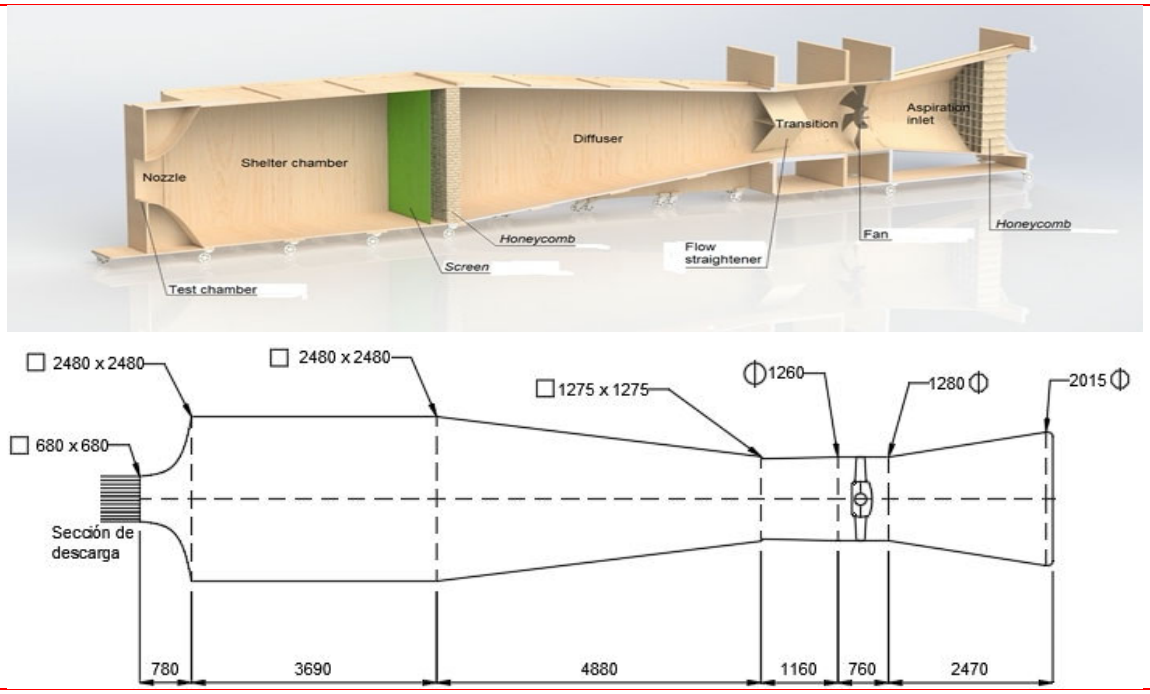

Fig. 3 Overview (up) and elevation (down) of the wind tunnel EB40-oWT

The meaning of the reduced frequency (ω^*) is analogous to that of the Strouhal number, except the former is relative to the natural frequency of the structure without flow effects and the latter is relative to the characteristic frequency of the aerodynamic phenomena.

A conventional inspectional analysis of the basic flow equations can be used to deduce dependence relationships among those dimensionless parameters. In particular the magnitude of the aerodynamic forces as well as the characteristic frequency of the fluid-dynamic excitation, which are represented by C_T and St, can be considered to be dependent on the other four parameters, Eqs. (8)-(9)

$$C_T = f(Re, C_K, \omega^*, \xi) \quad (8)$$

$$St = f(Re, C_K, \omega^*, \xi) \quad (9)$$

Therefore, if a prototype and a scaled model possessed the same values for those four dimensionless numbers, then the aerodynamic phenomena of interest would verify the conditions for similarity, and hence the parameters C_T and St of the scaled model would be equal to those of the prototype.

Regarding wind tunnel tests on reduced scale models, however, trying to impose exact similarity for the Reynolds number is usually incompatible with similarity for the other dimensionless parameters. Nonetheless, in this specific case the most important aerodynamic effects can be assumed to be related to dynamic bluff body separation and subsequent vortex shedding, rather than to boundary layer development and detachment. Because of that, the influence of the Reynolds number can be expected to be very small, especially when dealing with fully developed turbulent flows, and the Reynolds condition can be relaxed.

Hence, the design of the scale model should ensure that the other three dimensionless numbers, C_K, ω^* and ξ, are equal to those of the prototype. In the case of the damping ratio (ξ), that condition (Eq. 10) can be achieved by selecting materials with adequate mechanical properties, Eq. (10).

$$\xi_m = \xi_p \quad (10)$$

The moments of inertia of model and prototype are related through the length and density ratios. If their densities are equal, then the moment of inertia of the scale model must verify Eq. (11)

$$I_m = I_p \left(\frac{L_m}{L_p}\right)^5 \quad (11)$$

Identity of the torsional stiffness coefficient (C_K) between prototype and scale model brings about the following condition for the torsional stiffness of the model

$$K_m = K_p \left(\frac{U_m}{U_p}\right)^2 \left(\frac{L_m}{L_p}\right)^3 \quad (12)$$

Eq (12) allows to determine the flow velocity to be imposed in wind tunnel on the scale model for given values of the torsional stiffness. And the latter can be conveniently modified by changing the shaft material or varying its diameter and thickness. In this way, there is a certain freedom between the scale and the torsional stiffness ratio in the model and prototype.

2.2 Wind tunnel and instrumentation

The experimental tests were developed in the aerodynamic wind tunnel denoted as EB40-oWT, which is

located at the Energy Department building of the University of Oviedo. It is an open wind tunnel, the maximum air velocity at the test section is 35 m/s, the nominal power is 30 kW, 14.25 m in length and a test cross section of 0.68 x 0.68 m2. Fig. 3 reproduces the elements of the wind tunnel. Other details as well as nozzle assembling can be seen in Rodríguez-Lastra *et al.* (2013).

Figs. 4 (a)-(b) show the velocity profile (U/U_{max}) and turbulence intensity (TI) at the nozzle outlet of the wind tunnel. They correspond to the mid vertical plane and have been plotted as a function of the vertical coordinate y/z, with z = height of the nozzle outlet. Note that the same distribution is obtained in the mid horizontal plane due to the symmetry of the nozzle. It can be seen that the velocity profile is mostly uniform, since velocity values are higher than 98% of the maximum velocity except at the first 10 mm, which correspond to the thin boundary layer developed on the bottom surface. Besides, the turbulence intensity is below 1.7% except for the first 15 mm above the side and bottom walls.

For the current tests, the scale models were placed close to that bottom wall to resemble the proximity of the floor in real situations, but nonetheless the tracker board was well within the zone of uniform speed and turbulence.

During the tests, two main variables were measured: the rotation amplitude at the free end of the tracker and the torque at the driver, which was located at the other end.

For the rotation measurements, digital photography and video were used, together with an image analysis software. Video recording speeds of 300 and 1000 frames per second were used for the unsteady measurements. The estimated accuracy of the angle measurement was 1 degree.

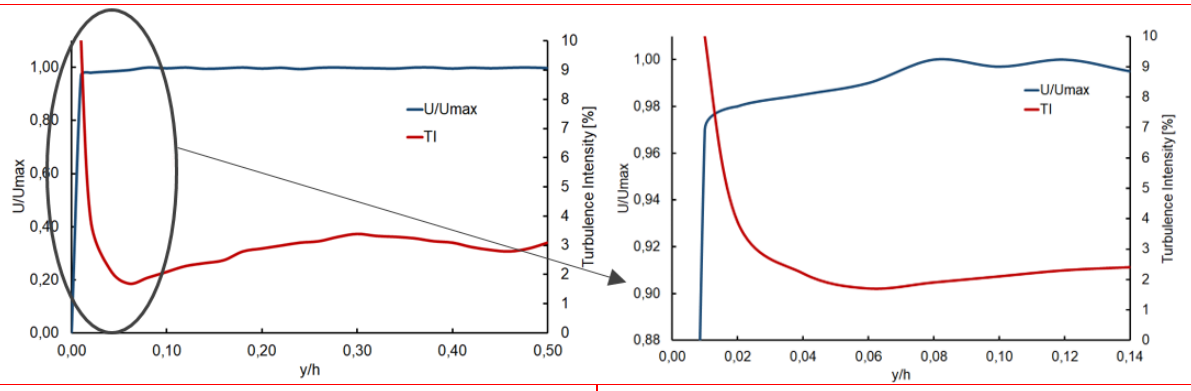

(a) Low half section | (b) Detail on bottom wall (boundary layer effect)

Fig. 4 Profiles of velocity and turbulence intensity at the nozzle outlet (vertical direction)

The torque at the driver was measured with a torsion balance that has an accuracy better than 1%, and a signal acquisition system whose frequency range is above 1 kHz.

2.3 Solar tracker scale models

The single-axis solar tracker prototype under study has the usual arrangement for this kind of structures, with the dimensions shown in the Table 1.

The torsion values of the structure are determined only by the shaft because the stiffness of the panel has little influence on this property of the structure (Katariya and Panda 2019, Aydogdu *et al*. 2018, Ebrahimi *et al*. 2020).

However, the inertia of the system comes determined by the surface and cross section of the panels because the shaft mass is small and concentrated on the axis.

Table 1 Prototype solar tracker dimensions

Description	Value
Tracker shaft length [m]	30
Shaft diameter [m]	0.2100
Shaft thickness [mm]	6
Shaft stiffness [Nm]	113450
Inertia [kg·m²]	1668
Panel chord [m]	3
Panel thickness [m]	0.0135

The solar tracker is supported by four pillars and the height from the torsional axis respect to the floor is 20% bigger than half the panel chord.

Fig. 5 shows an experimental model installed on the test section. Considering the symmetry of the solar tracker, the experimental model represents only half of the structure from the driver (fixed end) to the free end. In order to take full advantage of the test section, the scale is 1/45, meaning a blockage below 7 or 8% in any tilt position.

The models have been built mostly with PLA material, using additive manufacturing technologies. Table 2 contains the main information of the scaled structure.

Two types of models have been employed. Both have the same features except for the torsional stiffness of their shaft, in order to study its influence on the critical velocity. One is made of steel, resulting in a torsional stiffness K=0.2 N·m, and the other is made of brass, giving K= 0.092 N·m. Table 3 collects the properties based on the type of shaft.

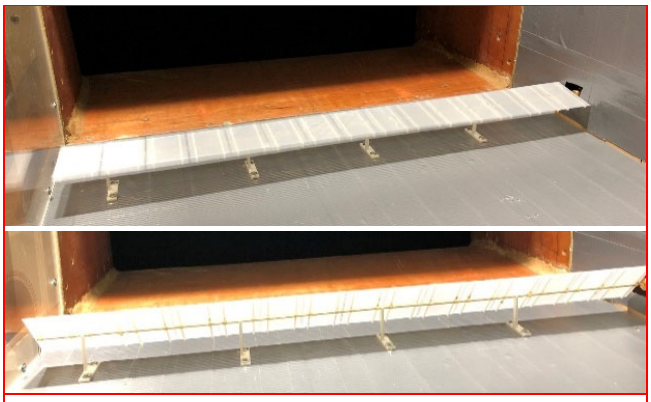

Fig. 5 Aeroelastic scale model

Table 2 Solar tracker model: main geometrical dimensions of panels and supports

Description	Value
Tracker shaft length [m]	0.670
Panel chord [m]	0.067
Support height [m]	0.040
Purlin thickness [m]	0.003

Table 3 Structural properties of models with different shafts

Concept	Brass	Steel
K[Nm]	0.092	0.200
I [kg·m²]	9.02e-6	9.02e-6
ξ [%]	1.600	2.400
ω_n[Hz]	25.300	37.000

Impact tests were performed to obtain the natural frequencies and damping ratio of the models. As an example, Fig. 6 shows a typical time signal of the drive torque after an initial displacement under no airflow conditions, exhibiting an amplitude decay from which the damping coefficient can be obtained.

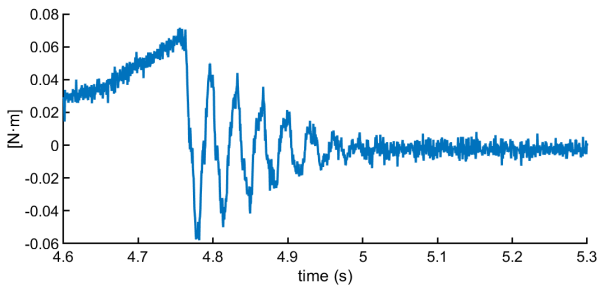

Fig. 6 Torque signal at the driver (fixed) section (impact test)

Fig. 7 presents the frequency spectrum of the torque signal from another impact test. The peak at 37 Hz, the one with highest amplitude, corresponds to the main natural frequency of the structure with the steel shaft. The logarithmic scale used for the torque axis allows to appreciate that there is also low amplitude excitation at higher frequencies, which are associated to harmonics of the first natural frequency and, to a lesser extent, to higher order vibration modes.

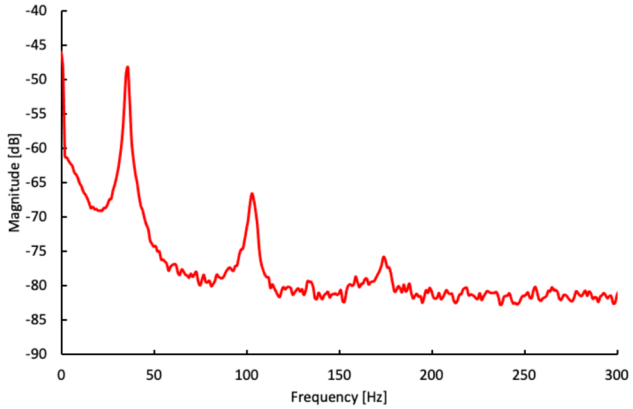

Fig. 7 Frequency spectrum of torque signal (impact test)

Since the inertia of the structure is uniformly distributed along the axis, the natural frequencies of the vibration correspond to the expression shown in Eq. (13) (Rao 2007, see Mohammadnejad 2015 for a more precise calculation)

$$\omega_n = \frac{(2n+1)\pi}{2}\sqrt{\frac{K}{I}} \quad (13)$$

3. Experimental results

In this section, experimental tests are explained and further discussed.

3.1 Description and classification of the phenomenon

According to different models tested, as the velocity increases, small vibrations can occasionally be observed, maybe due to turbulence or to sporadic vortex separation. Anyway, these are normally random and small amplitude oscillations. Nevertheless, a much more intense vibration develops from a certain velocity upwards.

Figs. 8-9 show the oscillations of the models under the wind load. As will be discussed below, these oscillations are believed to correspond to the phenomenon of torsional galloping, or one degree of freedom (1DOF) torsional flutter.

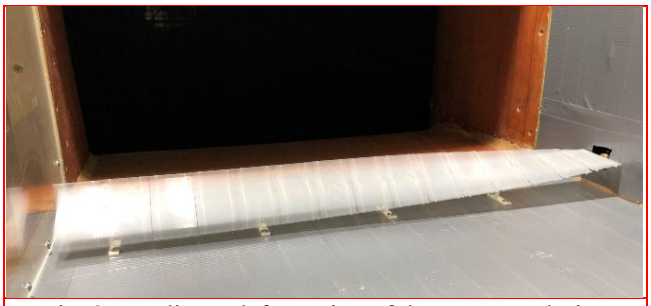

Fig. 8 Non-linear deformation of the structure during torsional galloping

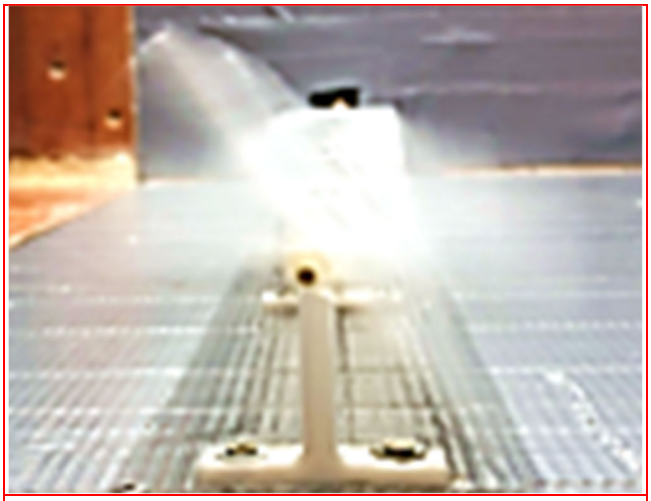

Fig. 9 Oscillation of the free end of the panel during torsional galloping

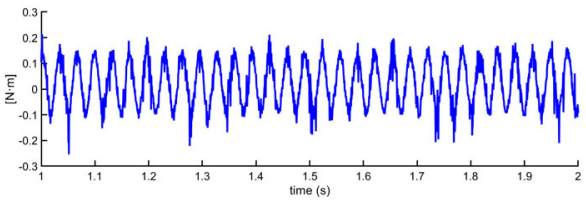

Fig. 10 Torque at the driver section of the scale model during the torsional galloping (tilt angle 20º and wind velocity 9.2 m/s)

As stated in the Section 2, it has been possible to measure the angles rotated by the free end of the tracker and the torque on the driver. For instance, Fig.10 shows the time signal of the torque during a galloping event. It corresponds to the tracker at a tilt angle of 20° and a 9.2 m/s wind speed. In this case, the amplitude of the torque oscillation is about five times greater than the average value. The average value is roughly speaking the one supported by the tracker just before galloping.

Fig. 11 depicts the FFT of the time signal. The main frequency of the oscillation is somewhat less than the first natural frequency of torsion of the tracker structure (due to the added aerodynamic stiffness). Also, for this case, the free end average angle is about 27º, seven more degrees than on the driver. The amplitude is about 72º, from -9º to 63º.

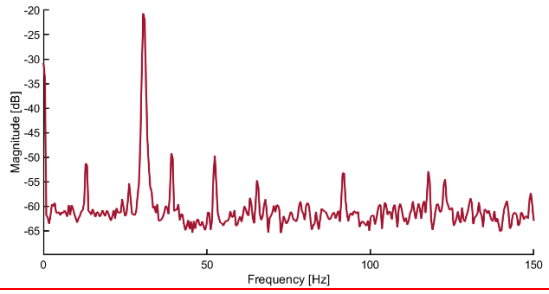

Fig. 11 Frequency analysis corresponding to the torque on the driver section of the scale model during the torsional galloping (tilt angle 20º and wind velocity 9.2 m/s)

This phenomenon seems to be caused by the aeroelastic interaction of vortex shedding at the leading and trailing edges of the panel, and the torsion of the structure. In simplified terms, vortex shedding causes the torque to fluctuate and the panel to rotate cyclically on its axis. At the same time, when the amplitude of the rotation is large enough, the oscillation of the panel causes the separation of the vortexes at the location of extreme rotations. In this way, the frequency of vortex separation is "locked in" to the natural frequency of the structure, and the fluid dynamic and mechanical phenomena feedback on each other.

As an example, in order to better understand and visualize the mechanism of the vortices that take part in the instability, Fig. 12 represents a numerical simulation of this phenomenon. The numerical model has been solved with the finite volume FLUENT code. It corresponds to an unsteady 2D simulation, including the ground effect. Up to 100.000 triangle unstructured cells have been used, together with a 0.001 s time step. The turbulence has been included using an RNG model and the boundary conditions were the atmospheric pressure and uniform velocity inlet (20 m/s in Fig. 12).

Essentially, the oscillation occurs centered on the original tilt angle and the separation of the vortices occurs near the location of extreme rotations. In a strong galloping there is vortex shedding at both the leading and trailing edges, although the one at the leading edge is larger and seems to be the main factor in the phenomenon (Rhor *et al.* 2015). In addition, some factors complicate even more the interaction of the flow and the motion of the structure. Consider, for example, that there is no symmetry between the top and bottom due to the tilt angle and the proximity of the ground.

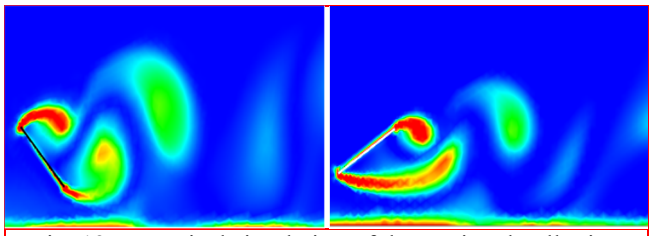

Fig. 12 Numerical simulation of the torsional galloping (contours of vorticity)

With regard to the identification of the phenomenon, its characteristics make it difficult to classify. On the one hand, torsional divergence, buffeting and wake induced vibrations can easily be ruled out: torsional divergence because it is a static phenomenon, the buffeting and the wake induced vibrations, because of the characteristics of the wind tunnel and because, as studied, the tracker would correspond to the first row in the column. This does not mean that these phenomena cannot be factors that facilitate the instability in subsequent rows.

On the other hand, the phenomenon seems to share some of the characteristics of vortex induced vibrations, flutter and galloping, although with reservations. With respect to the first one, as it has been commented, there is vortex shedding, but it does not behave like a bluff body. It has also been proven that it can be triggered at any speed that exceeds a certain value, regardless of the number of Strouhal.

Although the galloping is typically related to a bending movement, due to the stiffness of the cross section and changes in the lifting and drag forces during the rotation, this instability could be classified as a type of torsional galloping. However, it does not correspond to the formulas defined in the standards for this phenomenon (see, for example, Eurocode: EN1991-1-4 - Annex E: Vortex shedding and aeroelastic instabilities). Furthermore, the galloping should respond in a linear manner with the damping but, as it will be seen, this does not seem to be the case.

The similarity to flutter lies in the feedback between the deformation and the fluid dynamic forces produced by the air. Classical flutter requires the interaction of torsion and bending, and here there is no appreciable deformation, either along the longitudinal axis, or in the cross section. However, it is admitted that there are other types of flutter (Simiu and Scanlan 1996). For instance, as the field of aeronautics states, stall flutter bending is of little importance with respect to torsion. The difference with the behavior of this instability in wings and blades is that the flow separation is more like vortex shedding than a normal airfoil stall.

In view of the above, this phenomenon could be classified as a special type of one degree of freedom torsional flutter. Despite that, some authors prefer to refer to this phenomenon as torsional galloping, and that seems to be the most accepted name in the industry.

3.2 Critical velocity of the torsional galloping

Fig. 13 shows the behavior of the free end of the tracker (with a horizontal starting position, 0º tilt angle) as a function of speed. This behavior is directly related to the momentum in the driver by the stiffness of the structure. The mean value of the angle at the free end of the tracker and the amplitude of the oscillation over this mean value are depicted.

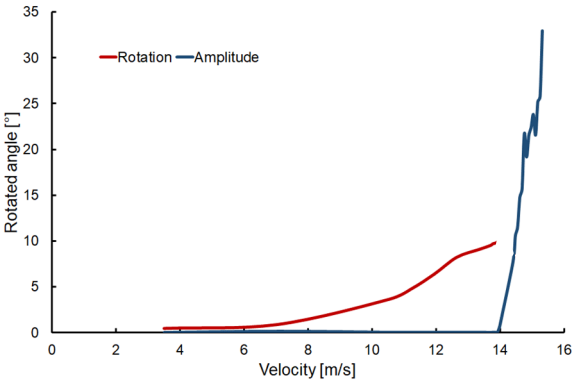

Fig. 13 Mean rotation and amplitude of the angular oscillation at the free end (tilt angle 0º)

Up to a speed of about 14 m/s, there is no oscillation, and the angle at the free end increases with speed as the wind load distributed along the tracker increases. The torsional deformation of the torque tube allows a relatively small rotation of the whole board (the PV panels) from the drive end to the free end.

When the instability identified as torsional galloping begins, an oscillation is produced, with an amplitude that grows very fast with the wind speed. The amplitude of the oscillation varies along the axis of the solar tracker from zero at the driver section to its maximum value at the free end, producing a longitudinal sinusoidal twist of the panel (in contrast with a linear distribution when the momentum is concentrated on the free end), see Fig. 14.

In the beginning of the oscillation, the amplitude could be small but, when the velocity increases, the amplitude intensifies exponentially. If the solar tracker is maintained in the range of oscillations of small amplitude, fatigue effects may appear in the structure. However, with a small increase in the wind velocity, larger amplitudes will appear, generating loads on the structure (much higher than the static and dynamic loads usually considered), and the solar tracker easily reaches structural collapse.

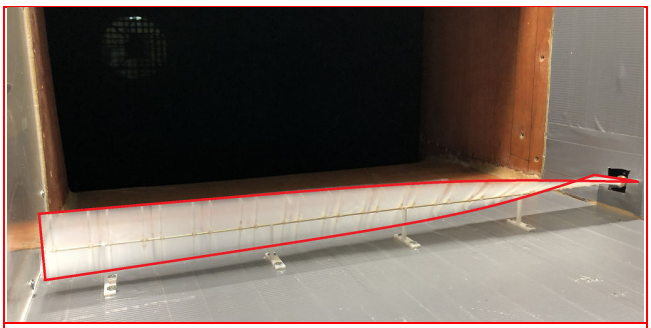

Fig. 14 Shaft's twist of the full aeroelastic scale model during torsional galloping

For this research, the most important part of the wind tunnel tests is to find the critical velocity at which the torsional galloping phenomenon appears.

The critical galloping velocity (U_{cr}) is taken from the speed at which the galloping can be triggered, whatever the cause or source of the initial instability that generates the aeroelastic event. Fig. 13 illustrates the sudden increase in the amplitude of the oscillation from 13.9 m/s onward. Due to the slope at this point (about 21º per m/s), the precision with which this speed can be determined is greater than 1%.

It has been found that, sometimes, the start of galloping can be delayed to speeds somewhat above critical, although when it falls into galloping, it goes directly into the oscillations of that higher speed. This effect is thought to be related to friction in the supports and increases if there are bending loads due to misalignments of the torque tube. However, that this delay is seen to be reduced if there is greater turbulence in the flow or if the tracker experiences a forced oscillation.

To avoid these effects and to find the minimum possible speed for the start of the galloping, the following experimental procedure has been followed: for each test, the speed is increased until the tracker goes into advanced galloping; from then on, the speed is reduced until the oscillation disappears. It has been found that, when approaching this point with the tracker oscillating, when it stops vibrating, it does not fall back into galloping, neither by increasing the turbulence, nor in the presence of gusts, nor even with externally forced oscillations.

The critical velocity depends on the tilt angle of the solar tracker. The entire speed range has been examined until instability is found, and measurements have been made for all angular tilts (from +75° to -75°) every 5°, and every 1º in the area near the horizontal. This has also allowed a detailed study around the classic stow positions, close to 0º tilt. Fig. 15 shows the found values, expressed as non-dimensional reduced velocity, in the so-called Stability Diagram:

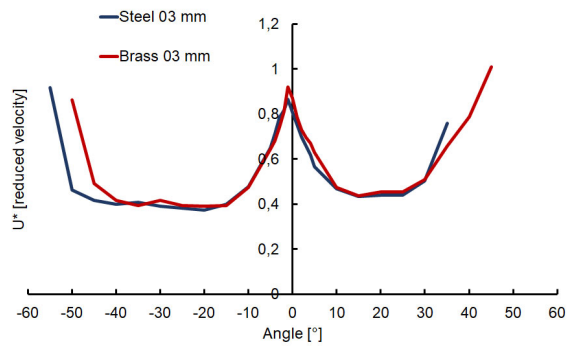

Fig. 15 Stability Diagram. Critical reduced velocity as a function of the tilt angles

The reduced velocity corresponds to the dimensionless wind speed taking into account the chord and the natural frequency (radians/s), Eq. (14):

$$U^* = \frac{U}{b}\frac{2}{\pi}\sqrt{\frac{I}{K}} \quad (14)$$

The oscillation phenomenon does not appear on every tilt angle, it is restricted between approximately +50° and -55° degrees. The minimum critical velocities show up in the range of -45° to -15° and from 20° to 40°, this velocity is more or less uniform in these ranges, with a value of 0.37 on the negative side and 0.43 for the positive one. For tilt angles close to zero, the critical velocities are higher, up to 0.86 for an angle of -1°. The maximum value is not zero centered at zero due to the asymmetry induced by the ground. The critical velocities also increase at the extremal angles (± 50°), where the forced oscillation disappears.

The plot behavior shows several aspects of the phenomenon:

- Considering the stable velocity on the angles ranging from -45° to -15° and from 20° to 40°, it seems to indicate that a certain kinetic energy is necessary for the oscillatory phenomenon to develop.
- For small tilt angles, between approximately -10° and +5°, the critical velocity is considerably higher. It is known that a flat plate with small angles of inclination does not shows the vortex shedding phenomenon (Blevins 1990). However, due to the flexibility of the structure, as the velocity increases, the angle of the free end deviates with respect to the end of the driver; the higher the velocity, the bigger the difference. For example, if the tilt position of the model solar tracker is 5°, when the wind velocity is 10 m/s, the free end angle is about 8°or 9°. What it means is that vortex shedding can be triggered on the free end with a velocity high enough, even at small tilt angles. It may be assumed that, if this velocity is sufficient for the necessary kinetic energy, the tracker will then go into the torsional galloping phenomenon.
- When the absolute value of the azimuthal angles is high enough, the torsional galloping phenomenon does not activate. It is possible that the flow detachment at the leading or trailing edge close to the ground may be much less energetic and is not sufficient to develop the instability. Or perhaps, the lack of symmetry makes more difficult the beginning of the instability.

Another aspect of the experimental results is that the values for the critical reduced velocity are basically the same on the two tested models in spite of the difference of the shaft's torsional stiffness (K). This is believed to be a consequence of the reduced velocity maintaining the dimensionless torsional stiffness coefficient (C_k). In other words, both tests keep the similarity with respect to the stiffness.

Only models with the same value of moment of inertia (I) have been tested, so it is still unknown its possible effect on the galloping critical velocity.

The damping ratio (ξ) values in both models are quiter different but both are also quite small. Although not included in this work, other tests with different materials have been carried out, and the preliminary results corroborate the idea that, when the damping ratio is small, it has little influence

on the onset of torsional galloping.

4. Discussion

4.1 Design values of wind speed and stiffness of the torque tube

The previous analysis and experimental results allow to calculate the maximum wind velocity that a specific prototype of solar tracker will stand before the onset of the torsional galloping.

For instance, for the prototype of solar tracker in this study, if the threshold value of the critical reduced velocity is set to 0.37, the galloping critical velocity is, Eq. (15)

$$U_{cr} = U_{cr}^{*} \cdot \frac{b \cdot \pi}{2} \cdot \sqrt{\frac{K}{I}} \approx 14.4\ m/s \quad (15)$$

Alternatively, it is also possible to calculate the shaft stiffness for a specified critical galloping velocity or maximum project wind speed, for example, for 100 km/h, as shown in Eq. (16)

$$K_{cr} = \frac{U_{cr}^{2}}{U_{cr}^{*2}} \frac{4I}{b^{2}\pi^{2}} = \approx\ 423356\ Nm \quad (16)$$

Which corresponds to a shaft thickness of 33 mm, instead of the 6 mm of the original prototype.

Normally, operation procedure in a photovoltaic facility calls for the solar tracker to assume a stow position when the wind is above a certain value; usually zero or a slightly negative tilt angle. In this case, the critical reduced velocity can reach a value around 0.8. This corresponds to a galloping critical velocity of 31 m/s, for the original prototype, or for a shaft thickness of 5 mm to withstand up to 100 km/h.

4.2 Critical velocity of the torsional galloping

The data in Fig. 15 are considered conservative, and suitable for this tracker (and any other fitting the similarity laws) with a uniform, steady and frontal wind. Based on this, some considerations can be made about other aspects that have influence on this problem.

The real wind is not uniform and continuous. Depending on the weather or the terrain conditions, there may be a strong influence of turbulence and gusts (buffeting). As mentioned above, the experimental procedure followed in this research ensures that no continuous galloping occurs if the wind speed is below the critical velocity. However, the absence of transient vibrations is not guaranteed. Due to this, the presence of strong turbulence or gusts may make it necessary to increase the design speed (Jia 2011).

An analogous reasoning can be made for the atmospheric boundary layer. Its presence decreases the average speed at the height of the tracker, so - in theory - the design speed of torsional galloping could be decreased (Fan 2020). However, in the boundary layer there may be more turbulence, and it may also be highly variable with weather conditions. This may make it convenient to take the design speed at a certain height above the trackers.

Regarding the position of the tracker in the row, the scale model is located in the tunnel between two walls, which makes it equivalent to an interior tracker. Some tests have been done with a tracker where the free end does not have an adjacent wall, which would be equivalent to a position at the end of the row. It has been found that, under these conditions, the edge effects cause the oscillation to be slightly reduced and the critical velocity to increase. The critical velocity data obtained would be on the safety side for these trackers.

No wind direction tests have been performed. It has been assumed that the most severe effects occur when considering the wind speed normal to the tracker, but this factor deserves further investigation.

As mentioned above, the studied tracker would correspond to a tracker in the front row. On the one hand these are the most exposed trackers but, on the other hand, the behavior of one row can affect the following ones.

The performance of a multi-row system, as designed for solar plants, is currently being tested. It has been found that if there are two rows of trackers, under some singular conditions, the second one may fall into galloping before the first one starts to oscillate. It needs further study, but this is believed to occur when the trackers are in a position close to horizontal, where the critical velocity is higher. Under these circumstances, the first tracker can change the angle of the flow over the second tracker to an area with a lower critical velocity in the Stability Diagram.

In any case, if the critical velocity is less than the minimum possible (according to Fig. 15), they should not reach the galloping, at least not continuously.

However, this may indicate that a stow position close to the horizontal may not be a good method to consider higher critical velocities than the minimum.

Apart from the above, the wake of the trackers may generate buffeting or wake induced vibrations in the rear rows, but that is outside the scope of this study.

5. Conclusions

An analytical and experimental analysis of the aeroelastic instabilities of a single-axis solar tracker has been carried out. The analytical procedure has led to identify and evaluate the dimensionless variables most relevant for the phenomenon. Based on this study, several aeroelastic scale models have been designed, built and tested in a wind tunnel. The models have been able to reproduce the phenomenon of torsional galloping that appears when wind velocities reach relatively high values.

- The results suggest that in order for torsional galloping to occur, two conditions must be met: the angle of the solar tracker has to be adequate for vortex shedding; and the flow must have a certain minimum kinetic energy.
- The measurements have allow to determine the galloping critical velocities for the whole practical range of tilt (azimuthal) positions.
- It has been found that the critical reduced velocity

for instability exhibits a minimum that changes little on a wide range of the tilt angle. That minimum can be set as a limit for stable operation.

- The stability range is higher when the tilt is close to horizontal since the critical velocity increases significantly. In addition, there are certain positive and negative tilt angles from which the instability no longer develops.
- The threshold value of the reduced critical velocity has been used to determine the wind speed at which aeroelastic instabilities start to develop, as well as the necessary shaft thickness for a given project wind speed.
- The results of the critical velocity have been obtained for a continuous, uniform and frontal wind speed. The experimental procedure allows to assume that those values are on the safety side to prevent torsional galloping with respect to the effects of other factors such as the atmospheric boundary layer, turbulence and gusts. However, configurations of multi-row trackers need to be further investigated. Also, the data found is only valid for the tracker studied, and those that meet the conditions of similarity.

Acknowledgments

This research has been developed in the framework of the FC-GRUPIN- IDI/2018/000205 project, supported by the Principado de Asturias – Plan de Ciencia, Tecnología e Innovación-, co-financed by FEDER funds.

Notations

b	Panel chord
c	Structural damping
C_k	Torsional stiffness coefficient
C_T	Torque coefficient
f,g	Function of
h	Height -equal to width- of the test section
I	Moment of inertia respect to the axis
K	Tracker torsional stiffness
L	Structure characteristic length
Re	Reynolds number
St	Strouhal number
T	Torque magnitude
TI	Turbulence intensity
U	Wind velocity
y	Height from the ground at the test section
θ	Angle
μ	Air dynamic viscosity
ρ	Air density
ξ	Damping ratio
ω	Frequency
Subscripts	
cr	critical
m	model
max	maximum
n	cycles number
p	prototype
Superscripts	
*	reduced

References

Aydogdu, M., Arda, M. and Filiz, S. (2018), "Vibration of axially functionally graded nano rods and beams with a variable nonlocal parameter", Adv. Nano Res., 6(3), 257-278. https://doi.org/10.12989/anr.2018.6.3.257.

Blevins, R.D. (1990), *Flow-Induced Vibration*. 2nd ed., Van Nostrand Reinhold Co., New York, NY, USA.

Dyrbye, C. and Hansen, S.O. (1997), *Wind Loads on Structures*, John Wiley & Sons, Ltd., Baffins Lane Chichester, Sussex, UK.

Fan, X., Wang, Z., Chen, X., Wang, Y. and Tan, W. (2020), "Experimental investigation on flow-induced vibration of flexible multi cylinders in atmospheric boundary layer", *Int. J. Mech. Sci.*, **183**, 105815. https://doi.org/https://doi.org/10.1016/j.ijmecsci.2020.105815.

Jia, J. (2011), "Wind and structural modelling for an accurate fatigue life assessment of tubular structures", *Eng. Struct.*, **33**, 477–491. https://doi.org/https://doi.org/10.1016/j.engstruct.2010.11.004.

Jubayer, C.M. and Hangan, H. (2015), "Numerical simulation of wind effects on a stand-alone ground mounted Photovoltaic (PV) system", *J. Wind. Eng. Ind. Aerodyn.*, **134**, 1–37. https://doi.org/10.1016/j.jweia.2014.08.008.

Katariya, P.V. and Panda, S.K. (2019), "Numerical frequency analysis of skew sandwich layered composite shell structures under thermal environment including shear deformation effects", *Struct. Eng. Mech.*, **71**(6), 657–668. https://doi.org/10.12989/SEM.2019.71.6.657.

Lave, M. and Kleissl, J. (2011), "Optimum fixed orientations and benefits of tracking for capturing solar radiation in the continental", *Renew. Energy*, **36**, 1145–52. https://doi.org/10.1016/j.renene.2010.07.032.

Mohammadnejad, M. (2015), "A new analytical approach for determination of flexural, axial and torsional natural frequencies of beams", *Struct. Eng. Mech.*, **55**(3), 655–674. https://doi.org/10.12989/SEM.2015.55.3.655.

Païdoussis, M.P., Price, S.J. and De Langre, E. (2011), *Fluid Structure Interaction: Cross flow induced Instabilities*, Cambridge University Press, Cambridge, UK.

Rao, S.S. (2007), *Vibration of Continuous Systems*. Wiley, New York.

Rodríguez Lastra, M., Fernández Oro, J.M., Galdo Vega, M., Blanco Marigorta, E. and Santolaria Morros, C. (2013), "Novel design and experimental validation of a contraction nozzle for aerodynamic measurements in a subsonic wind tunnel", *J. Wind. Eng. Ind. Aerodyn.*, **118**,3 5–43. https://doi.org/10.1016/j.jweia.2013.04.008.

Roedel, A. and Upfill-Brown, S. (2018), "Designing for the Wind, using dynamic wind analysis and protective stow strategies to lower solar tracker lifetime costs". White Paper. NEXTracker.

Rohr, C., Bourke, P.A. and Banks, D. (2015), "Torsional instability of single-axis solar tracking systems", *Proc. 14th Int. Conf. Wind. Eng.*, Porto Alegre Brazil, June.

Simiu, E. and Scanlan, R.H. (1996), *Wind Effects on Structures: Fundamentals and applications to design*, 3th ed., John Wiley & Sons, Ltd., New York, NY, USA.

Strobel, K. and Banks, D. (2014), "Effects of vortex shedding in arrays of long inclined flat plates and ramifications for ground-mounted photovoltaic arrays", *J. Wind. Eng. Ind. Aerodyn.*, **133**,146–149. https://doi.org/10.1016/j.jweia.2014.06.013.

Talavera, D.L., Muñoz-Cerón, E., Ferrer-Rodríguez, J.P. and Pérez-Higueras, P.J. (2019), "Assessment of cost-competitiveness and profitability of fixed and tracking photovoltaic systems: the case of five specific sites", *Renew. Energy*, **134**, 902–913. https://doi.org/https://doi.org/10.1016/j.renene.2018.11.091.

Taylor, Z.J. and Browne, M.T.L. (2020), "Hybrid pressure integration and buffeting analysis for multi-row wind loading in an array of single-axis trackers", *J. Wind. Eng. Ind. Aerodyn.*, **197**, 104056. https://doi.org/10.1016/j.jweia.2019.104056.

Yang, Y. (2010), "Experimental Investigations of Vortex Induced Vibration of a Flat Plate in Pitch Oscillation", M.Eng. Dissertation, A&M University, Texas.